Electronic Supplementary Material (ESI) for Nanoscale.
This journal is © The Royal Society of Chemistry 2020

Electronic Supplementary Information

Construction of Series-Wound Architectures Composed of Metal–Organic Frameworks Derived Hetero-(CoFe)Se_2 Hollow Nanocubes Confined into Flexible Carbon Skeleton as Durable Sodium Storage Anode

Xiaoqing Ma [a, c†], Jie Chen [†d], Wenxi Zhao [b *]

[a.] School of Chemistry and Chemical Engineering,Yangtze Normal University, Fuling, Chongqing, 408100, P.R.China.

[b.] School of Electronic Information Engineering, Yangtze Normal University, Fuling, Chongqing, 408100, P.R.China.

[c.] Sports Medicine Center, Department of Orthopedic Surgery, Southwest Hospital, the 3rd Military Medical University, Chongqing 400038, China.

[d.] Institute for Clean Energy & Advanced Materials, Faculty of Materials and Energy, Southwest University, Chongqing 400715, P. R. China.

***Corresponding author:** Wenxi Zhao, E-mail: zwx.168@163.com

[†] **Those authors contributed equally to this work**

Experimental section

Synthesis of zeolitic imidazolate framework (ZIF-67) nanocubes. ZIF-67 nanocubes were constructed depending on the reference [1]. In brief, a light pink mixed solution composing of 0.584 g $Co(NO_3)_2 \cdot 6H_2O$ and 10 mg cetyltrimethylammonium bromide (CTAB) in 20 ml deionized water were rapidly added into the 140 ml aqueous solution containing 9.08 g 2-methylimidazole and continuous stirred for 30 min, and then the purple precipitate was obtained by means of filtration and cleaning using deionized water and ethanol several times.

Preparation of ZIF-67/Co-Fe Prussian blue analogue (PBA). Typically, the above prepared 0.22 g ZIF-67 nanocubes was dispersed in 150 ml ethanol and ultrasonic treatment for 30 min to form A solution. Meanwhile, 0.5 g $K_3[Fe(CN)_6]$ was dissolved in 50 mL deionized water to form B solution. And then, B solution was rapidly infunded into A solution to form a reddish brown mixture and continuous stirring for 5 h. Subsequently, the brick-red product was collected by filtration and cleaning using deionized water and ethanol several times.

Construction of hetero-(CoFe)Se_2@carbon nanofibers skeleton ((CoFe)Se_2@CNS). (CoFe)Se_2@CNS was constructed though carbon nanofibers skeleton wrapping hetero-(CoFe)Se_2 hollow nanocubes via electrospinning method. Typically, 0.32 g ZIF-67/Co-Fe PBA was dispersed into 6 ml N,N-dimethylformamide (DMF) solution containing 0.6 g of polyacrylonitrile (PAN, average M_w = 150000, Aldrich) and vigorous stirring for 12 h at 40 ^oC. And then, the above mixture was loaded into a 10 ml syringe, which was electrospun on the receiver (aluminum foil) at a flow velocity of about 1 ml h^{-1} with an applied voltage of 17 kV and distance parameters of 12 cm between the injector needle and the receiver. Afterwards, the collected precursor membrane was stabilized at 200 ^oC for 1 h followed by carbonization at 600 ^oC for 2 h in Ar atmosphere at a ramped rate of 2 ^oC min^{-1} to form Co_3O_4/Fe_3O_4@CNS. Finally, (CoFe)Se_2@CNS was obtained by selenization treatment with mass ration of Co_3O_4/Fe_3O_4@CNS vs selenium powder of about 1:2. For comparison, the pure (CoFe)Se_2 was prepared by selenizing ZIF-67/Co-Fe PBA at same selenyation route, while $CoSe_2$@CNS composites can be collected by replacing ZIF-67 with ZIF-67/Co-Fe under the same electrospinning conductions.

Synthesis of $Na_3V_2(PO_4)_3$/C. Na_3V_2 $(PO_4)_3$/C samples were synthesized based on the previous report [2]. In brief, a mixtures composing of 4.68 g $NaH_2PO_4 \bullet 2H_2O$, 1.49 g V_2O_3 (99.9%, Alpha) and 1 g sugar was put into an agate jar as precursors, which can be were ball-milled in a planetary

ball mill at 460 rpm in a stainless steel vessel for 8 h under an Ar atmosphere. Afterwards, the mixture was transferred into a tube furnace and kept a heating rate of 2 °C min^{-1} up to 800 °C for 24 h in an Ar atmosphere, forming the $Na_3V_2(PO_4)_3$/C compound.

Materials characterization

The phase structure and valence states of the samples were measured by X-ray diffraction (XRD) (Shimadzu XRD-7000 X-ray diffractometer) and X-ray photoelectron spectroscopy (XPS, ThermoFisher ESCALAB 250Xi). Morphological structures of the samples were carried out using field-emission scanning electron microscope (FESEM, JSM-6510F) and transmission electron microscope (TEM, FEI Tecnai G2F20). The carbon ration of the samples was determined using thermogravimetric analysis (TGA, TA Instruments, USA) though 30−700 °C with a heating rate of 10 °C min^{-1} in air. Raman spectra were performed on a Raman spectrometer (Horiba Scientific LabRAM HR Evolution) from 500 to 2500 cm^{-1} using a 532 nm laser excitation at room temperature.

Electrochemical measurements

The electrochemical behaviors of the samples in a standard CR2032 type coin cells were measured. The working electrode was fabricated by directly coating a copper collector with homogeneous slurry composed of 60% active material, 30% super P and 10 % carboxymethyl cellulose sodium (CMC). The mass loading of the active materials on each electrode is about 0.7-1 mg. Moreover, sodium metal, glass microfibers (Whatman, GF/D) together with 1 M $NaCF_3SO_3$ in diethyleneglycol dimethylether (DEGDME) was used as the counter electrode, separator and electrolyte, respectively. In addition, $Na_3V_2(PO_4)_3$/C electrode was prepared by casting slurries containing 70 wt% active materials, 20 wt% Super P, and 10 wt% polyvinylidene fluoride (PVDF) binder onto aluminum foil by a doctor blade method. Cyclic voltammetry (CV) tests using CHI660e electrochemical workstation were performed in a potential range of 0.5−3 V and electrochemical impedance spectroscopy (EIS) measurements in a frequency range from 0.01 Hz to 100 kHz were explored at the same environment conditions. Charging/discharging curves on a LAND CT2001A-type battery test system (Wuhan, China) were carried out. In addition, the excessive $Na_3V_2(PO_4)_3$/C cathode guarantees a full storage performance of the (CoFe)Se_2@CNS anode in a full SIBs cell. It needs to be emphasized that the mass ratio of $Na_3V_2(PO_4)_3$/C to (CoFe)Se_2@CNS is 6.0 ~ 8.0 in full cell systems. Meanwhile, the (CoFe)Se_2@CNS anode was

initial dis-/charged for 3 cycles at 0.1 A g^{-1} in half cells, which can be set for 12 h before be applied to full cell configuration. In addition, the electrochemical performance of sodium ion full cell configuration with the $Na_3V_2(PO_4)_3$/C cathode and (CoFe)Se_2@CNS anode was constructed in a standard electrolyte of 1M $NaPF_6$ in EC/DEC solution with 5 vol % FEC. For the measurement of ex-XRD and ex-XPS, the cycled electrodes at different de-/sodiated states were disassembled in an Ar-filled glove box and washed with DEGDME several times before testing, followed by the naturally dried in a glove box. Afterwards, the electrodes can be placed in an argon-filled centrifuge tube and sealed with parafilm in a glove box, which can be quickly transferred to the XRD and XPS equipment to further measure relevant features.

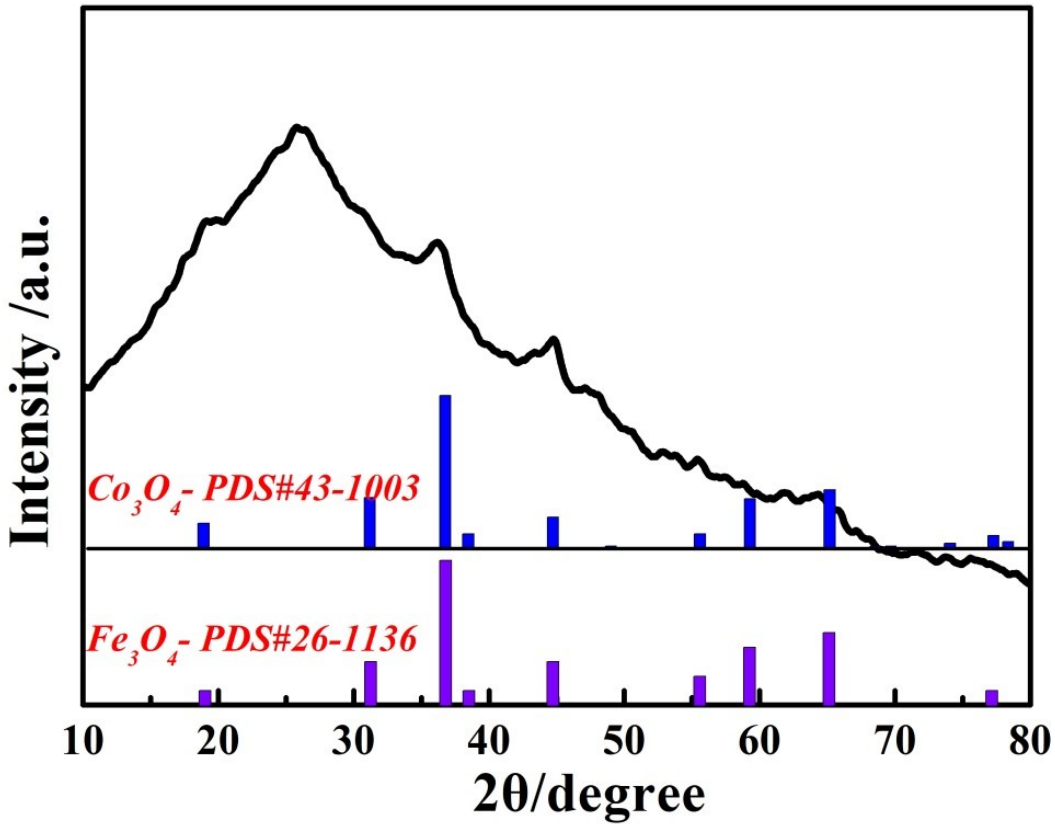

Fig. S1 XRD pattern of Co_3O_4/Fe_3O_4@CNS.

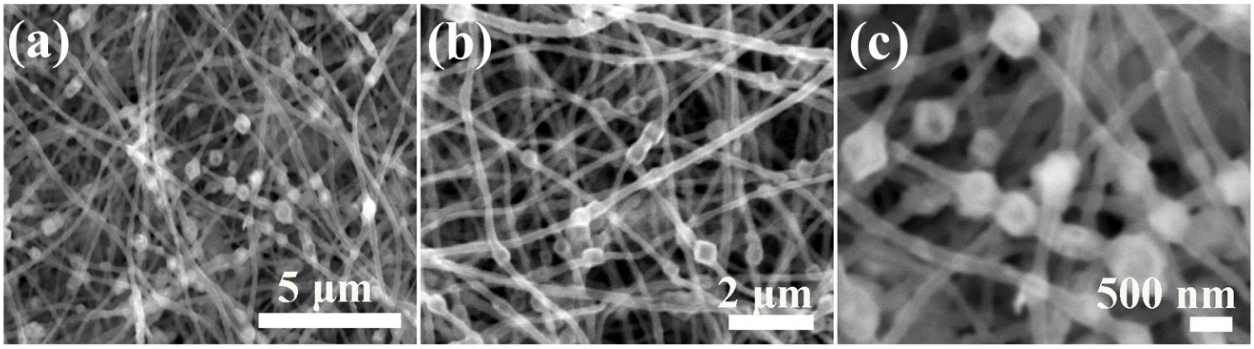

Fig. S2 Morphological SEM characterizations of the Co_3O_4/Fe_3O_3@CNS.

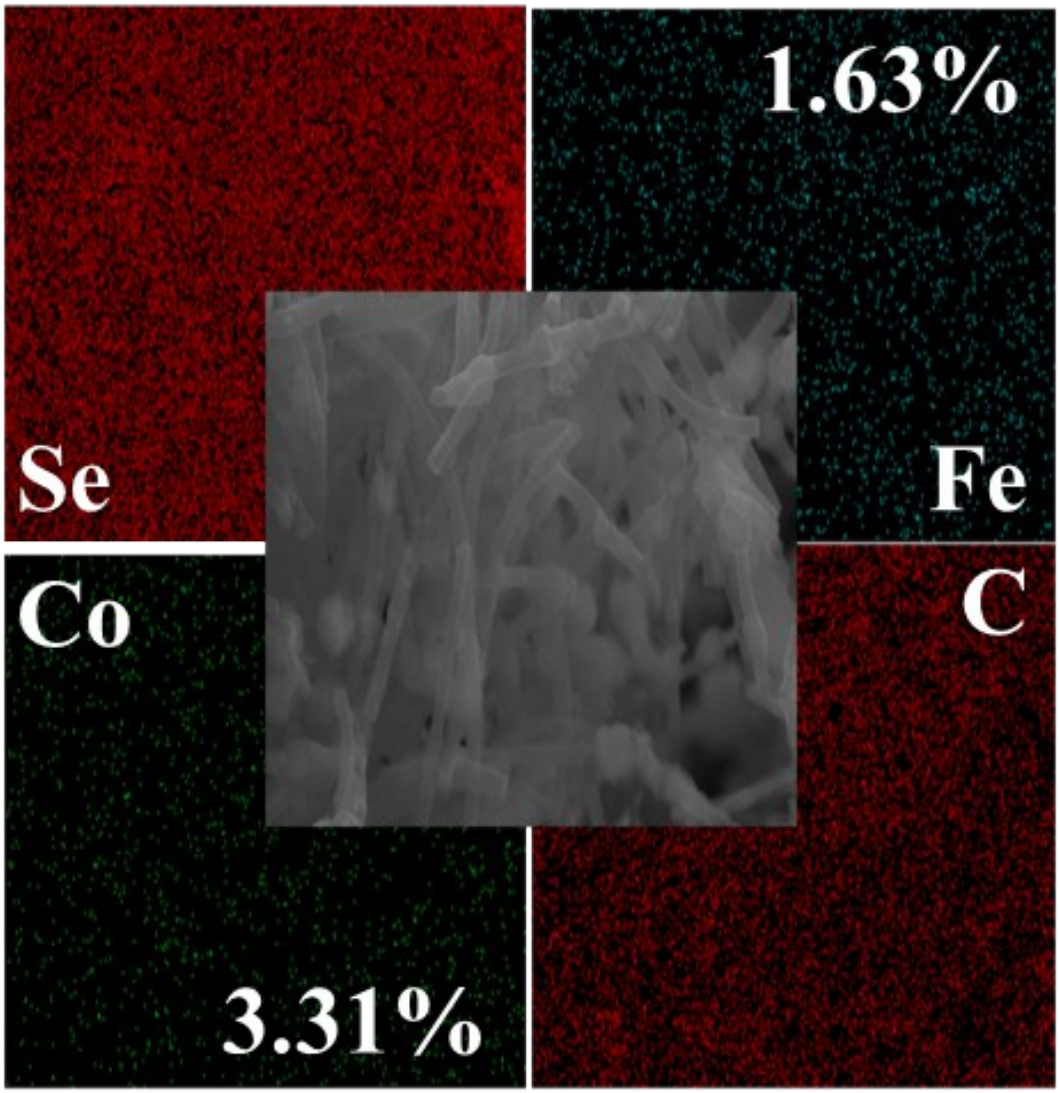

Fig. S3. The FESEM elemental mapping of $(CoFe)Se_2$@CNS.

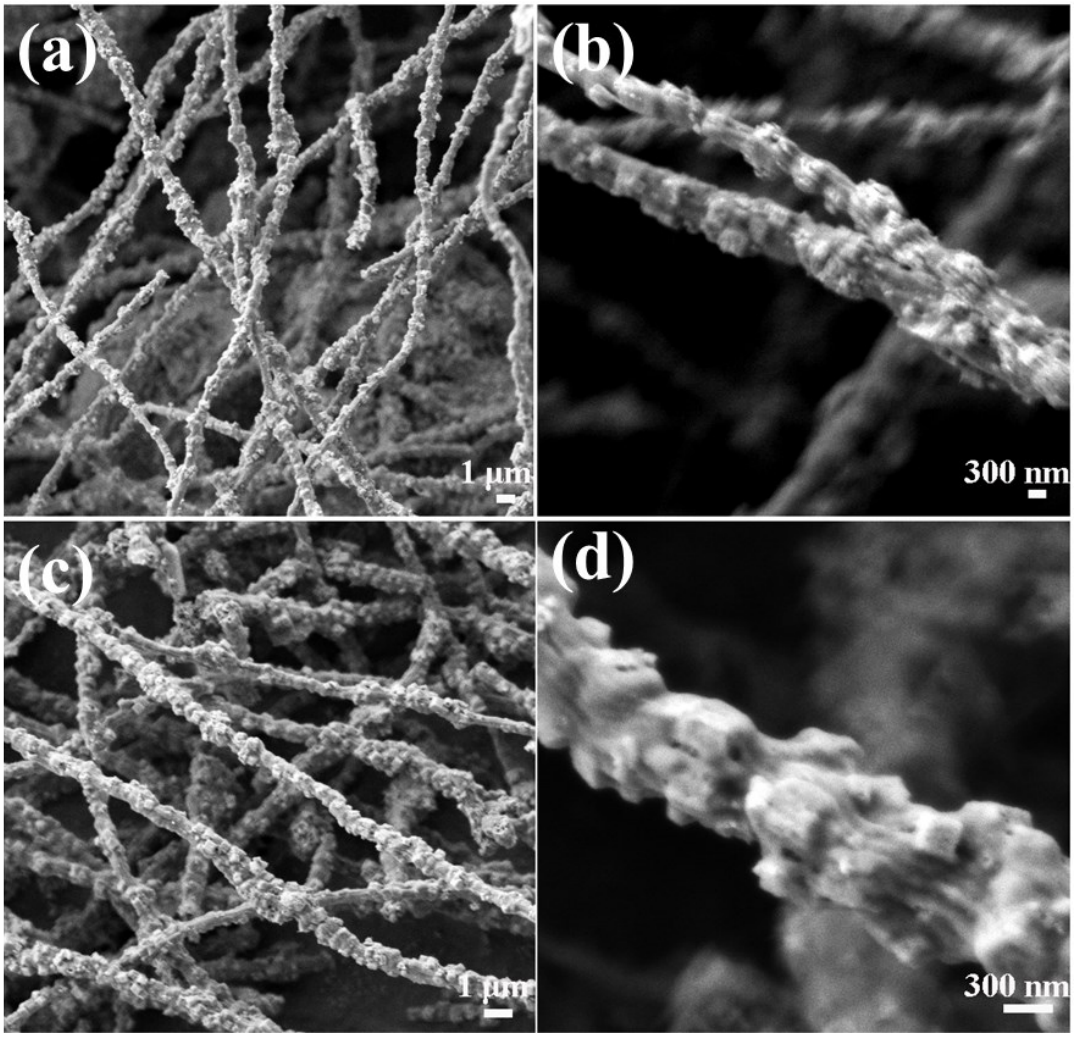

Fig. S4 SEM images of different $(CoFe)Se_2$@CNS composites: (a, b) 0.6 g $(CoFe)Se_2$ + 0.6 g PAN, (c, d) 0.72 g $(CoFe)Se_2$ + 0.6 g PAN.

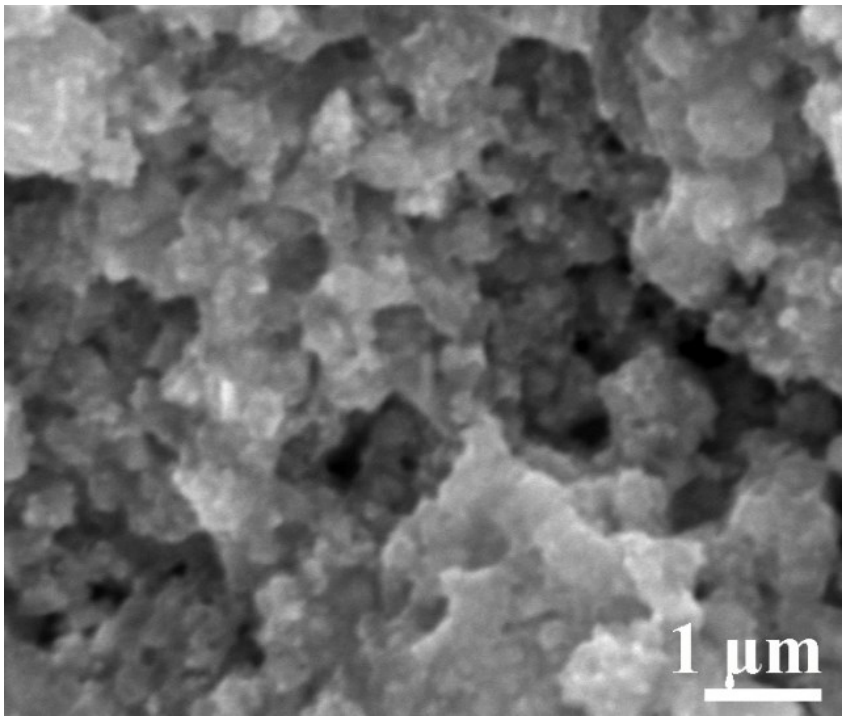

Fig. S5 SEM image of plain $(CoFe)Se_2$.

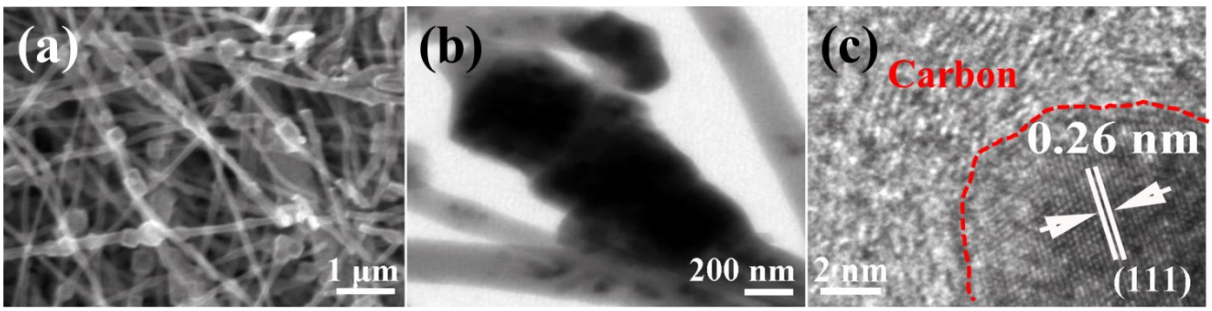

Fig.S6 SEM (a) and TEM (b) image of $CoSe_2$@CNS; (c) HR-TEM image of $CoSe_2$@CNS.

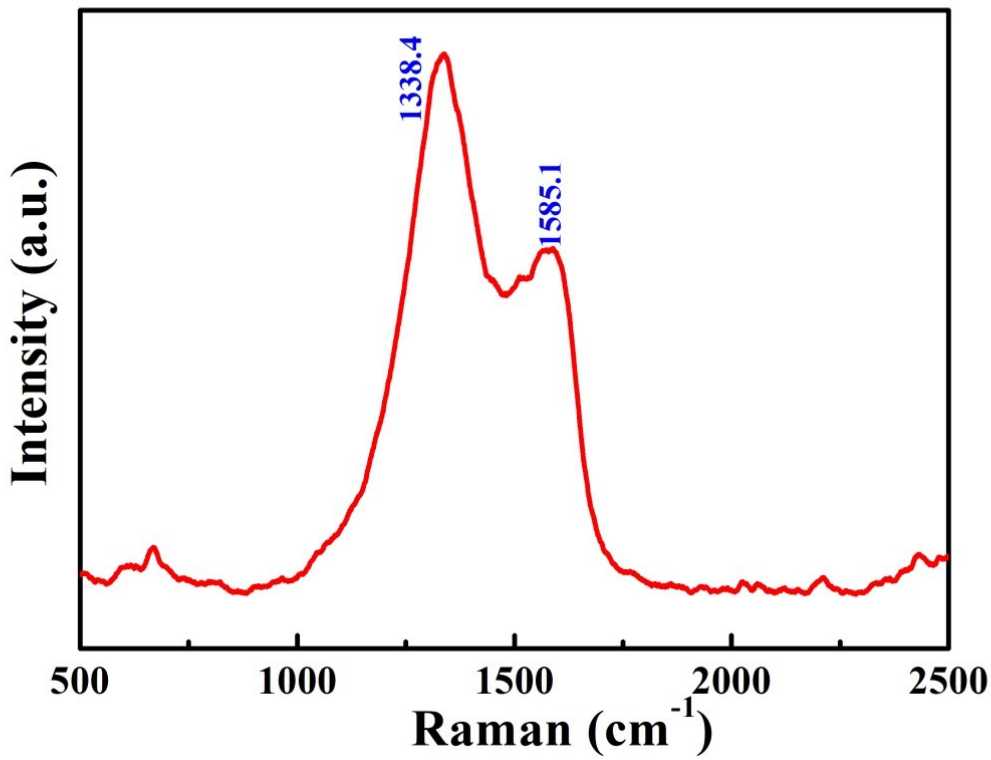

Fig. S7 Raman spectrum of (CoFe)Se_2@CNS.

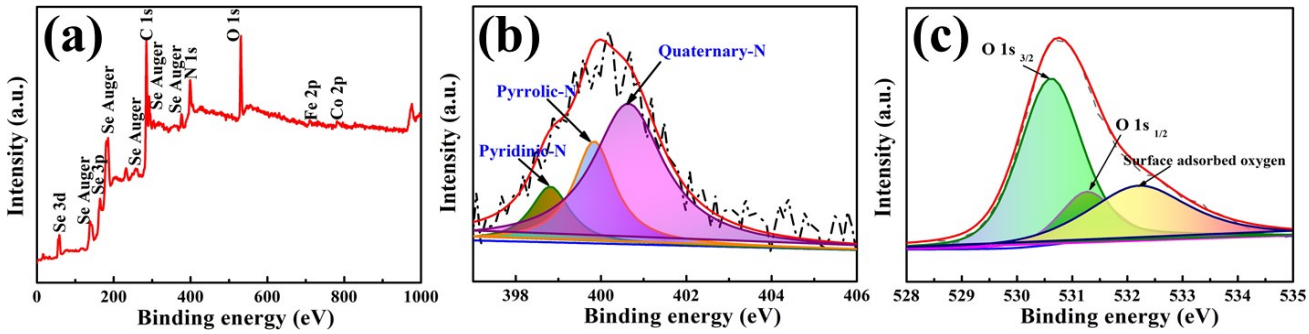

Fig.S8 (a) XPS survey spectrum of (CoFe)Se_2@CNS. High resolution XPS spectra, (b) N 1s; (c) O 1s.

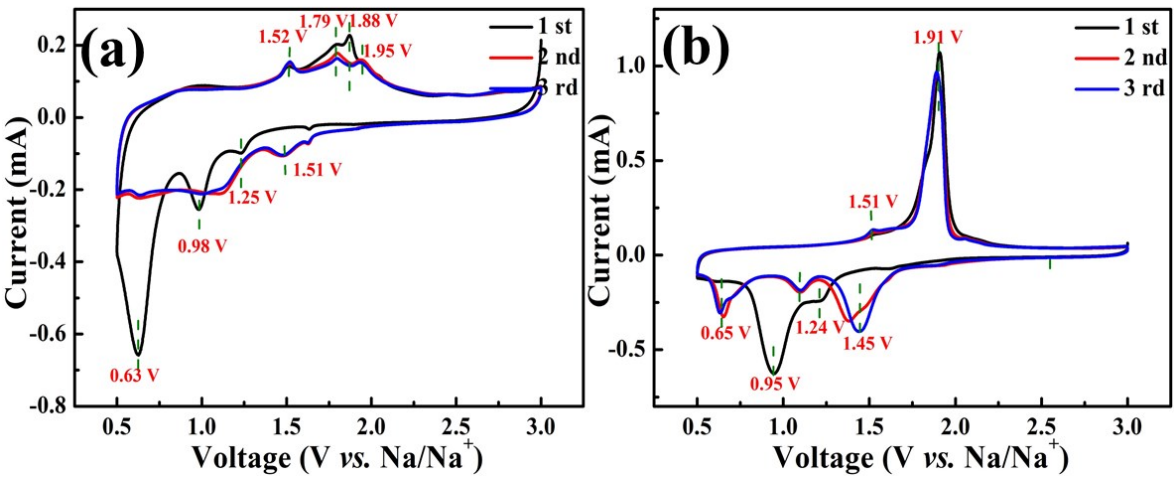

Fig. S9 CV curves of plain $(CoFe)Se_2$ (a) and $CoSe_2$@CNS (b) in a voltage ranging of 0.5-3.0 V at a scan rate of 0.5 mV s^{-1}.

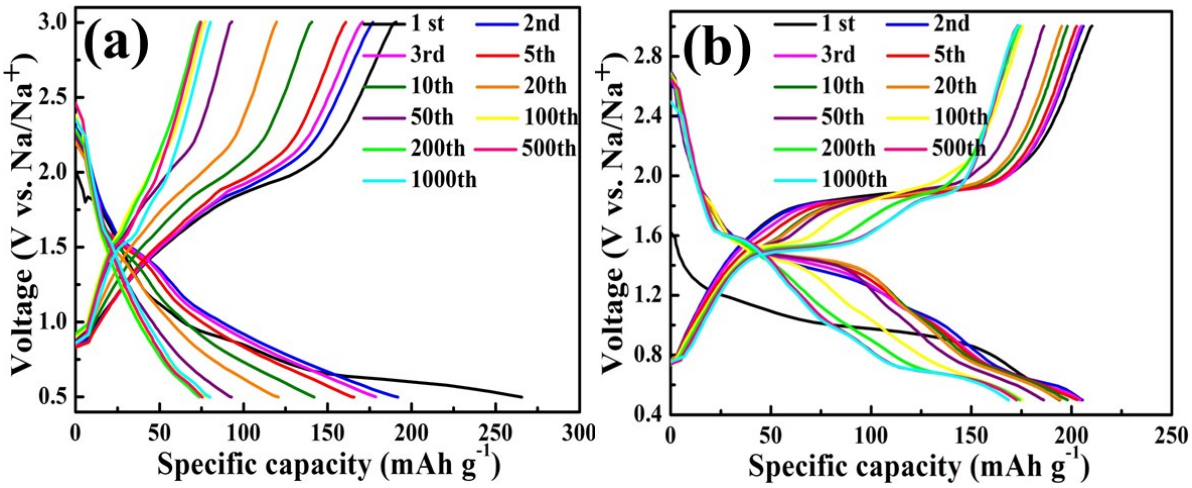

Fig. S10 Galvanostatic de-/sodiation voltage curves of plain $(CoFe)Se_2$ (a) and $CoSe_2$@CNS (b) at 2 A g^{-1}.

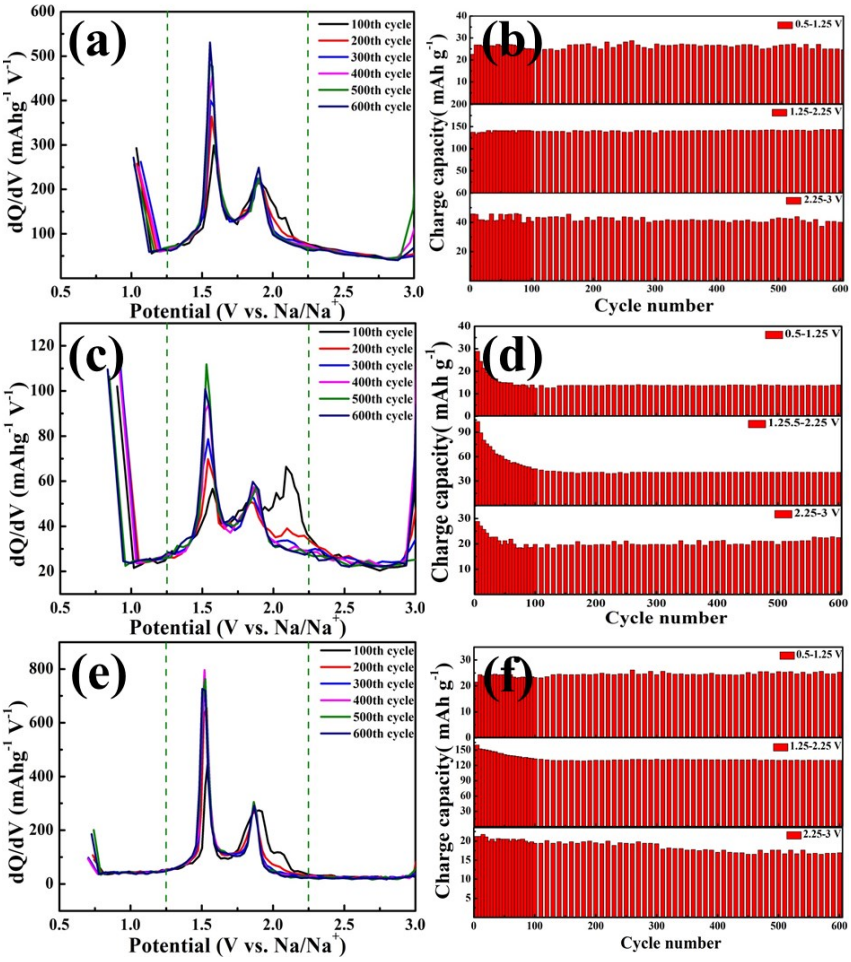

Fig.S11 Differential charge capacity profiles *versus* potential of $(CoFe)Se_2$@CNS (a), plain $(CoFe)Se_2$ (c) and $CoSe_2$@CNS (e) at different cycles; (d) Reversible charge capacities *versus* cycle number for the $(CoFe)Se_2$@CNS (b), plain $(CoFe)Se_2$ (d) and $CoSe_2$@CNS (f) at different voltage range at 2 A g^{-1}.

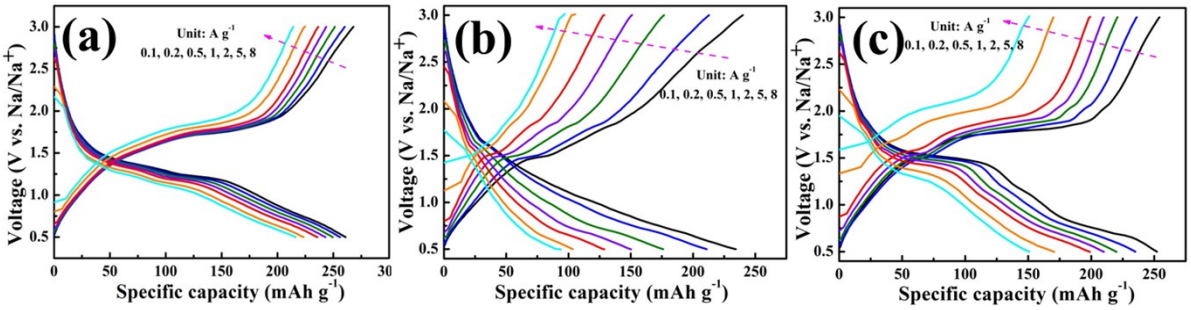

Fig. S12 Charge/discharge curves of $(CoFe)Se_2$@CNS (a), plain $(CoFe)Se_2$ (b) and $CoSe_2$@CNS (c) electrodes at various rates.

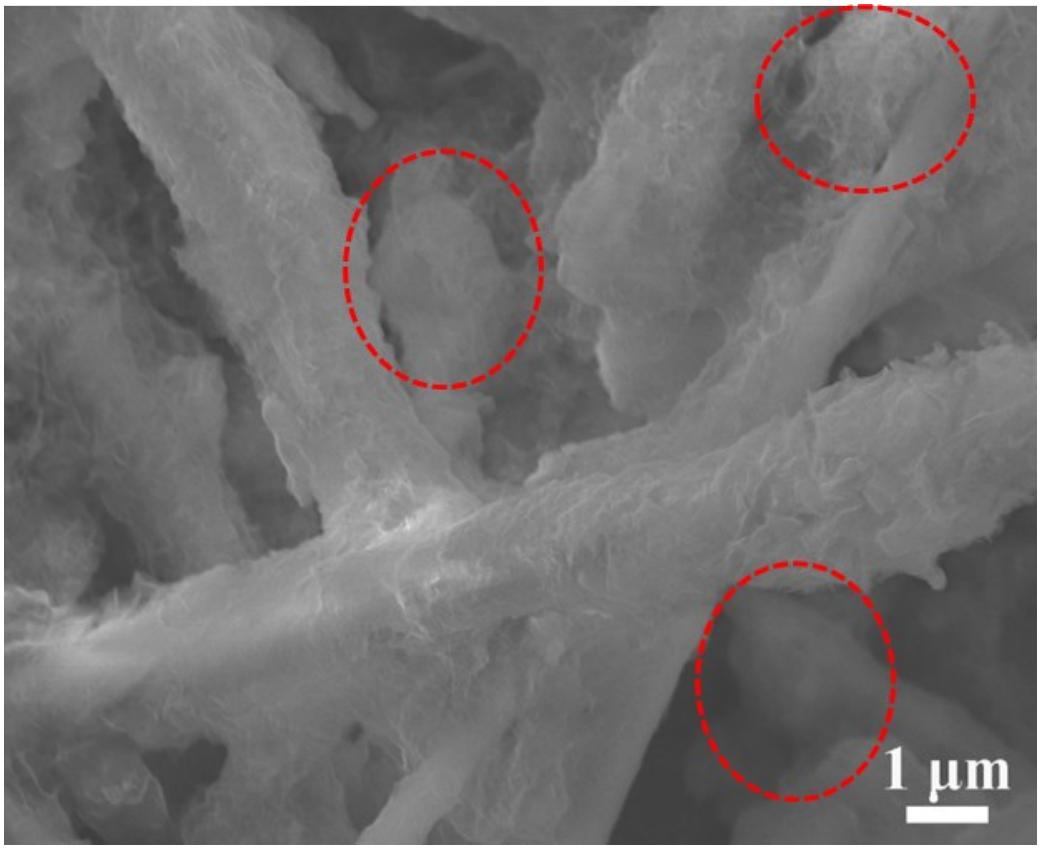

Fig. S13 FESEM image of (CoFe)Se_2@CNS electrode after 5630 cycles at 8 A g^{-1}.

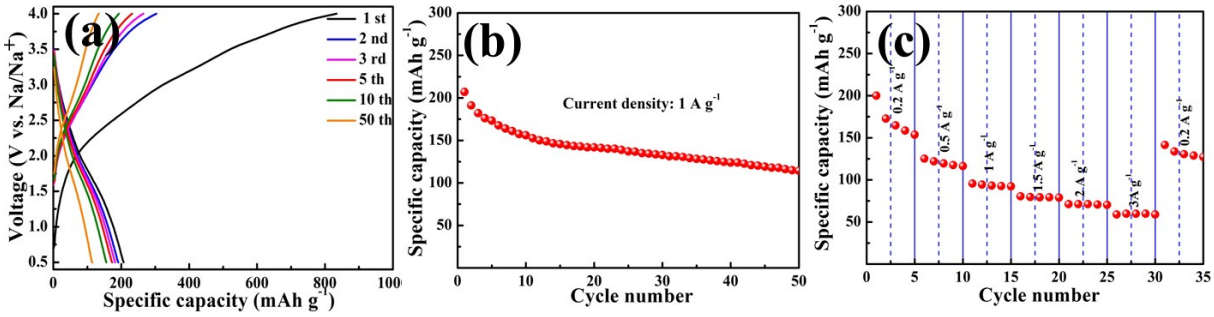

Fig. S14 Charge/discharge curves (a) and cycling stability (b) of sodium ion $Na_3V_2(PO_4)_3$/C//(CoFe)Se_2@CNS full cell at 1 A g^{-1}. (c) Rate performance of $Na_3V_2(PO_4)_3$/C//(CoFe)Se_2@CNS full cell at different rates.

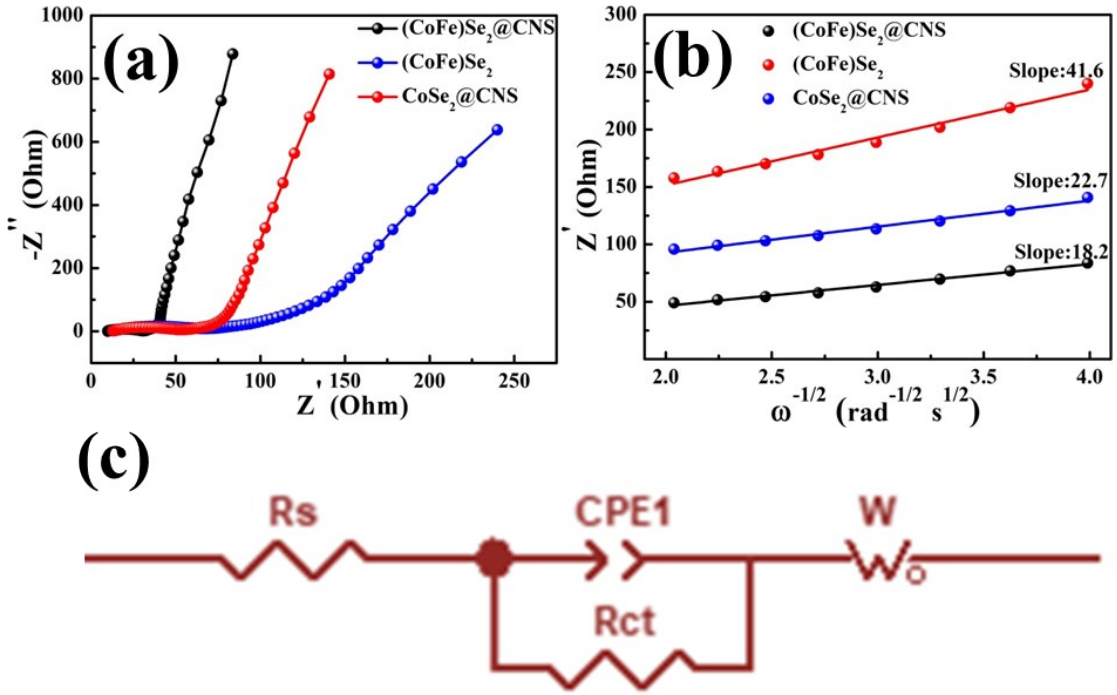

Fig. S15 Nyquist plots (a) and the corresponding linear relation of Z' vs. $\omega^{-1/2}$ (b) for (CoFe)Se_2@CNS, (CoFe)Se_2 and $CoSe_2$@CNS electrodes, (c) equivalent circuits for fitting the experimental EIS data for three electrodes.

Table S1 Fitting result of EIS spectra in Fig. S15 with the equivalent circuit proposed

Samples	**R_s(Ω)**	**R_{ct}(Ω)**	**σ (Ω cm^2 s^{-1})**	**D_{Na+} (cm^2 s^{-1})**
CoFe)Se_2@CNS	9.58	19.29	18.20	1.12×10^{-10}
(CoFe)Se_2	12.81	48.01	41.60	2.14×10^{-11}
$CoSe_2$@CNS	12.2	37.71	22.70	7.28×10^{-11}

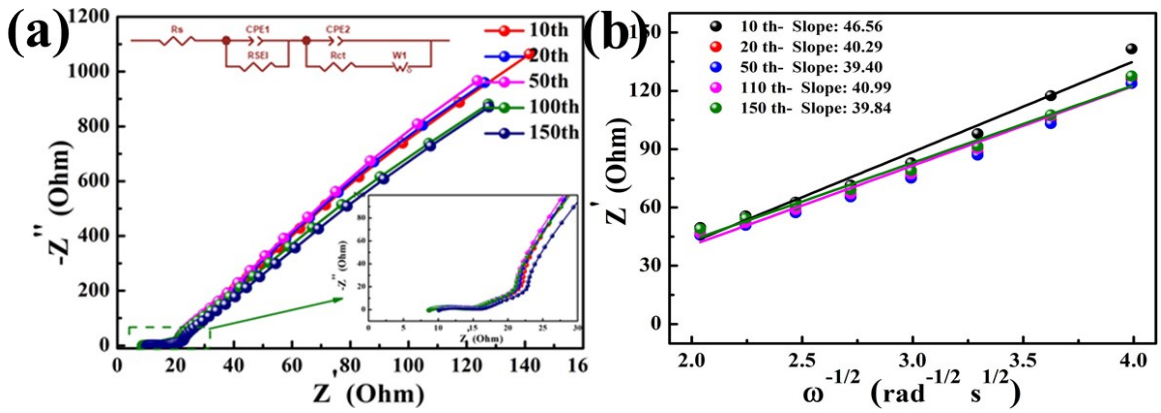

Fig.S16 Nyquist plots (a) and the corresponding linear relation of Z' vs. $\omega^{-1/2}$ (b) of (CoFe)Se_2@CNS electrode at different cycles.

Table S2 Fitting result of EIS spectra in Fig. S16 with the equivalent circuit proposed

Cycle number	R_s (Ω)	R_{ct} (Ω)	σ (Ω cm^2 s^{-1})
10th	8.88	3.70	46.56
20th	8.85	3.67	40.29
50th	8.96	3.23	39.40
100th	8.89	3.34	40.99
150th	10.37	3.38	39.84

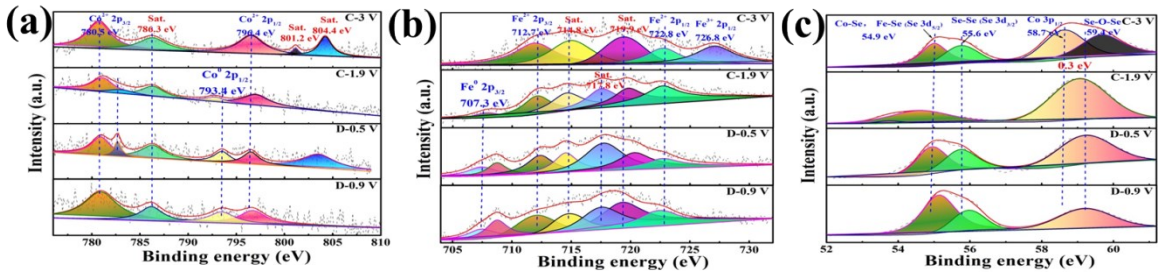

Fig. S17 Ex-situ XPS spectra of (CoFe)Se_2@CNS at different initial charge-discharge states: (a) high-resolution Co 2p spectra, (b) high-resolution Fe 2p spectra, (c) high-resolution Se 3d spectra;

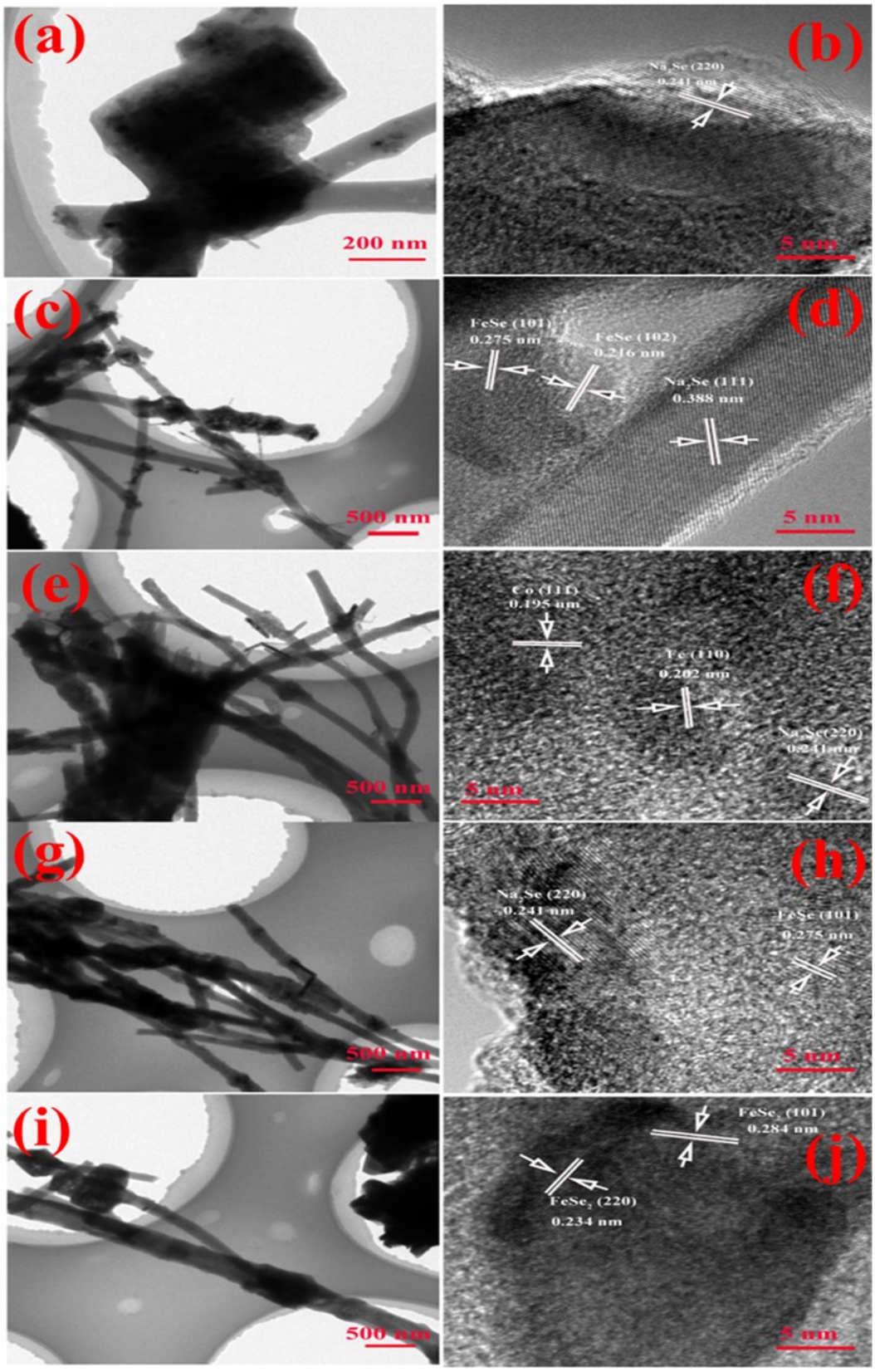

Fig. S18 TEM and HRTEM images of (CoFe)Se_2@CNS at different initial de-/sodiated states: (a, b) discharged to 1.3 V, (c, d) discharged to 0.9 V, (e, f) discharged to 0.5 V, (g, h) charged to 1.9 V, (i, j) discharged to 3.0 V.

Table S3 Fitting result of EIS spectra in Fig. 5c and 5e with the equivalent circuit proposed

Initial state	R_s (Ω)	R_{ct} (Ω)	σ (Ω cm^2 s^{-1})
D-1.3 V	8.46	11.85	78.50
D-0.9 V	8.55	11.52	50.10
D-0.7 V	8.48	9.40	22.90
D-0.5 V	8.36	6.98	18.60
C-1 V	8.36	9.97	19.30
C-1.5 V	8.26	13.08	46.10
C-1.9 V	7.75	13.27	76.80

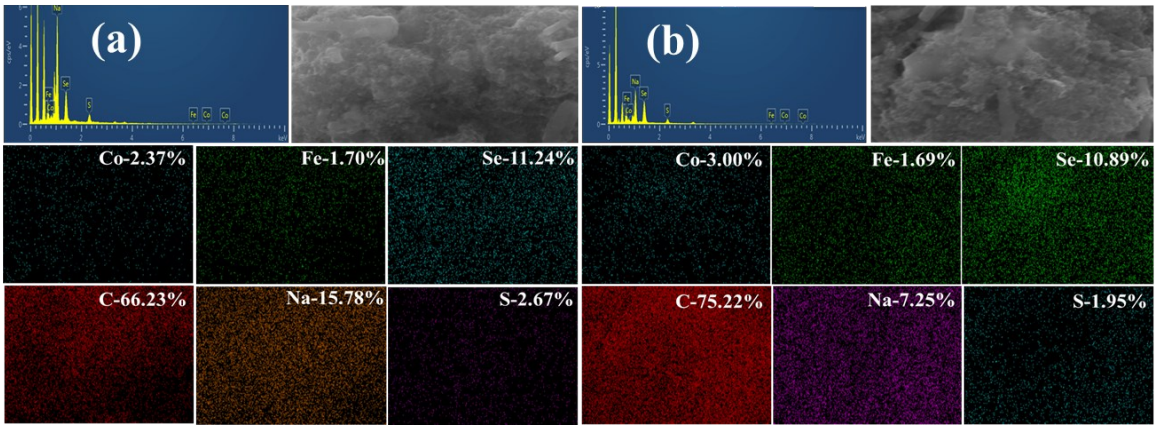

Fig. S19 The FESEM elemental mapping of (CoFe)Se_2@CNS at the initial cycle, (a) at fully discharged state of 0.5 V; (b) at fully charged state of 3 V.

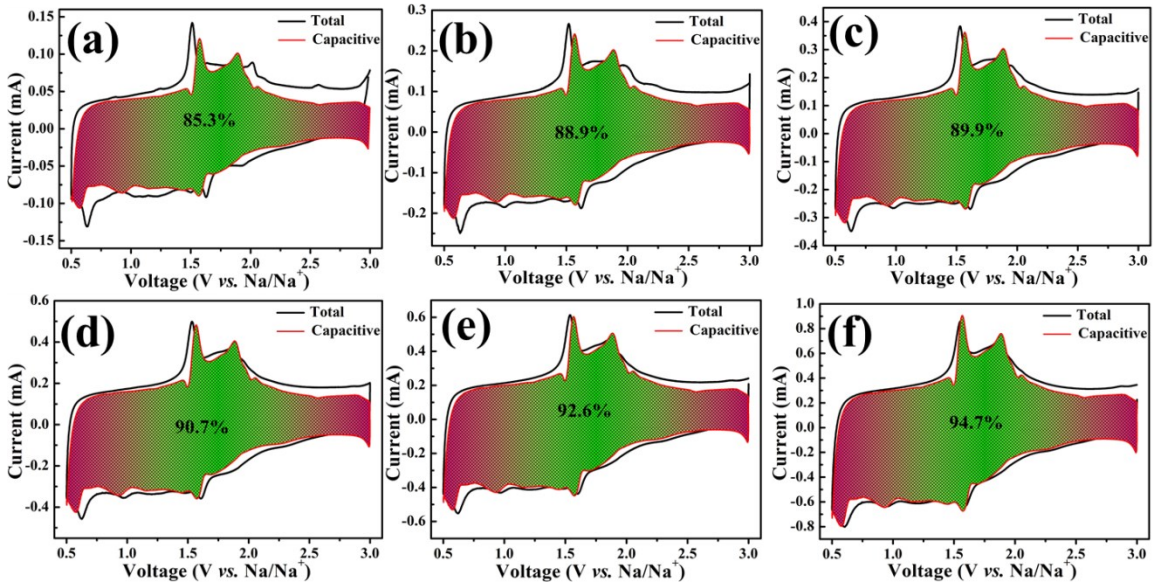

Fig. S20 The exact fraction of pseudocapacitive contributions for (CoFe)Se_2@CNS electrode shown by the shaded region at various scan rates: (a) 0.2 mV s^{-1}, (b) 0.4 mV s^{-1}, (c) 0.6 mV s^{-1}, (d) 0.8 mV s^{-1}, (e) 1 mV s^{-1}, (f) 1.5 mV s^{-1}.

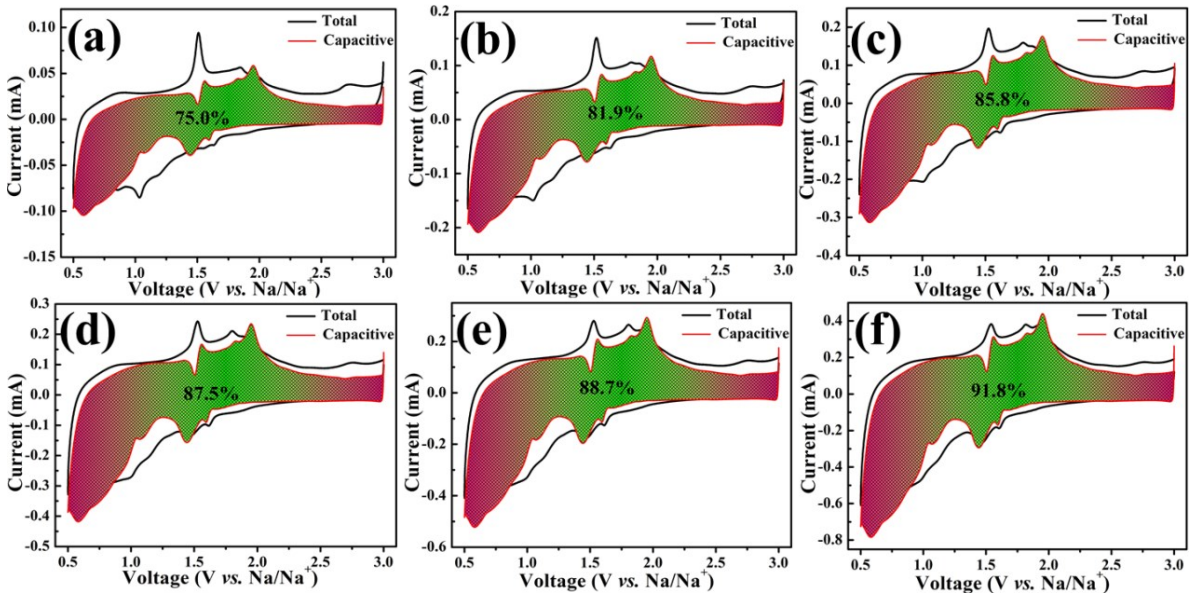

Fig. S21 The exact fraction of pseudocapacitive contributions for (CoFe)Se_2 electrode shown by the shaded region at various scan rates: (a) 0.2 mV s^{-1}, (b) 0.4 mV s^{-1}, (c) 0.6 mV s^{-1}, (d) 0.8 mV s^{-1}, (e) 1 mV s^{-1}, (f) 1.5 mV s^{-1}.

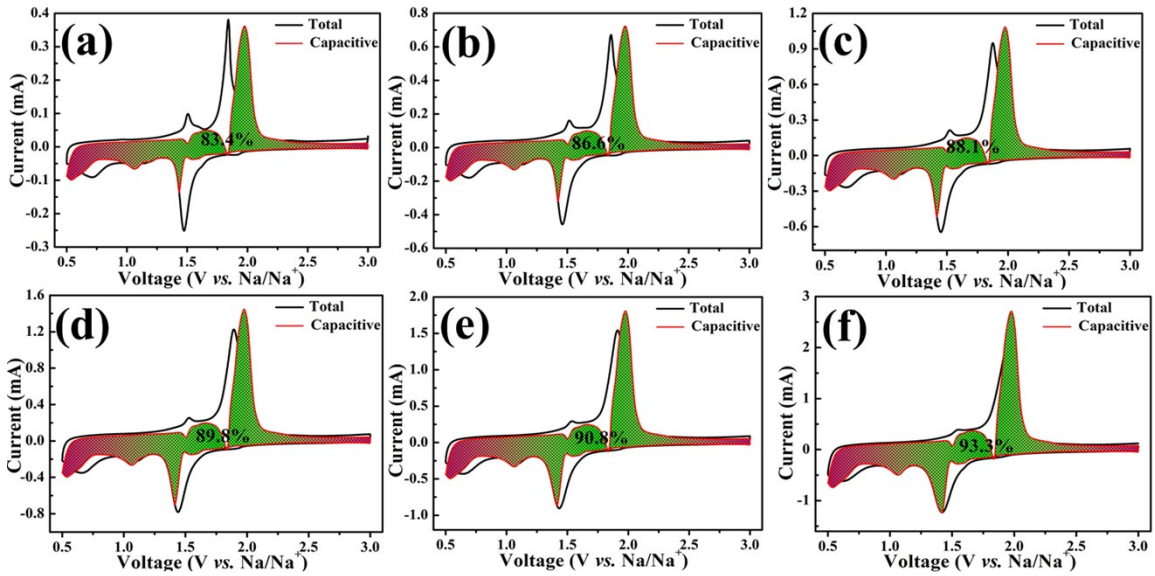

Fig. S22 The exact fraction of pseudocapacitive contributions for $CoSe_2$@CNS electrode shown by the shaded region at various scan rates: (a) 0.2 mV s^{-1}, (b) 0.4 mV s^{-1}, (c) 0.6 mV s^{-1}, (d) 0.8 mV s^{-1}, (e) 1 mV s^{-1}, (f) 1.5 mV s^{-1}.

References

[1] X. Wang, L. Yu, B. Yuan G., S. Y. Song, and X. Wen (David) Lou, Adv. Mater., 2018, 29, 1801211.

[2] Z. L. Jian, W. Z. Han, X. Lu, H. X. Yang, Y. S. Hu, J. Zhou, Z. B. Zhou, J. Q. Li, W. Chen, D. F. Chen, and L.Q. Chen, Adv. Energy Mater. 2013, 3, 156 – 160.